

## Subnatural-Linewidth Polarization-Entangled Photon Pairs with Controllable Temporal Length

Kaiyu Liao,<sup>1</sup> Hui Yan,<sup>1,\*</sup> Junyu He,<sup>1</sup> Shengwang Du,<sup>2</sup> Zhi-Ming Zhang,<sup>3</sup> and Shi-Liang Zhu<sup>4,1,5,†</sup>

<sup>1</sup>Laboratory of Quantum Engineering and Quantum Materials, School of Physics and Telecommunication Engineering, South China Normal University, Guangzhou 510006, China

<sup>2</sup>Department of Physics, The Hong Kong University of Science and Technology, Clear Water Bay, Kowloon, Hong Kong, China

<sup>3</sup>Laboratory of Quantum Engineering and Quantum Materials, School of Information and Photoelectronic Science and Engineering, South China Normal University, Guangzhou 510006, China

<sup>4</sup>National Laboratory of Solid State Microstructures, School of Physics, Nanjing University, Nanjing 210093, China

<sup>5</sup>Synergetic Innovation Center of Quantum Information and Quantum Physics, University of Science and Technology of China, Hefei 230026, China

(Received 11 February 2014; revised manuscript received 28 April 2014; published 20 June 2014)

We demonstrate an efficient experimental scheme for producing polarization-entangled photon pairs from spontaneous four-wave mixing (SFWM) in a laser-cooled <sup>85</sup>Rb atomic ensemble, with a bandwidth (as low as 0.8 MHz) much narrower than the rubidium atomic natural linewidth. By stabilizing the relative phase between the two SFWM paths in a Mach-Zehnder interferometer configuration, we are able to produce all four Bell states. These subnatural-linewidth photon pairs with polarization entanglement are ideal quantum information carriers for connecting remote atomic quantum nodes via efficient light-matter interaction in a photon-atom quantum network.

DOI: [10.1103/PhysRevLett.112.243602](https://doi.org/10.1103/PhysRevLett.112.243602)

PACS numbers: 42.50.Dv, 03.67.Bg, 42.65.Lm

The connectivity of a long-distance photon-atom quantum network strongly depends on efficient interactions between flying photonic quantum bits and local long-lived atomic matter nodes [1,2]. Such efficient quantum interfaces, which convert quantum states (such as time-frequency waveform and polarizations) between photons and atoms, require the photons to have a bandwidth sufficiently narrower than the natural linewidth of related atomic transitions (such as 6 MHz for rubidium *D1* and *D2* lines). As a standard method for producing entangled photons, spontaneous parametric down-conversion (SPDC) in a nonlinear crystal usually has a wide bandwidth (larger than terahertz) and very short coherence time (less than picosecond). Many efforts have been investigated in the past more than one decade ago to narrow down the SPDC photon bandwidth by using optical cavities [3–8]. However, the bandwidth of SPDC polarization-entangled photon pairs is still wider than most atomic transitions and leads to a very low efficiency of storing these polarization states in a quantum memory [5,9].

Our motivation was stimulated by the recent progress in generating subnatural-linewidth biphotons by using continuous-wave spontaneous four-wave mixing (SFWM) in a laser-cooled atomic ensemble with electromagnetically induced transparency (EIT) [10,11]. Photons produced from this method not only have narrow bandwidth but also automatically match the atomic transitions. The applications of these narrow-band photons include the demonstration of a single-photon memory with a storage efficiency of about 50% [12], a single-photon precursor [13], and coherent control of single-photon absorption and reemission [14]. However, while this method provides a natural entanglement

mechanism in the time-frequency domain, it is extremely difficult to produce polarization entanglement because of the polarization selectivity of EIT in a nonpolarized atomic medium [15]. It is possible to generate the polarization entanglement by scarifying the EIT effect, but the photon generation efficiency is low and the bandwidth is not narrower than the atomic natural linewidth [16]. The “writing-reading” technique with optical pumping provides a solution to polarization entanglement but results in reducing time-frequency entanglement [17].

In this Letter, we report our work on producing subnatural-linewidth polarization-entangled photon pairs by using the continuous-wave SFWM cold-atom EIT configuration. We demonstrate that the polarization entanglement can be efficiently produced by making use of a Mach-Zehnder interferometer in a two-path SFWM setup while maintaining the EIT effect in controlling the photon bandwidth. By tuning the phase difference between the two SFWM paths and properly setting the driving laser polarizations, we can generate all four Bell states. These photons have a coherence time of up to 900 ns and an estimated bandwidth of about 1 MHz that is much narrower than the Rb atomic natural linewidth (6 MHz). These subnatural-linewidth polarization-entangled photon pairs are ideal flying qubits for connecting remote atomic quantum nodes in a quantum network.

Our experimental setup is illustrated in Fig. 1. We work with a two-dimensional <sup>85</sup>Rb magneto-optical trap (MOT) with a longitudinal length of  $L = 1.7$  cm [18]. The experiment is run periodically. In each cycle, after 4.5 ms MOT time, the atoms are prepared in the ground level  $|1\rangle$  and followed by a 0.5 ms SFWM biphoton generation window.

Along the longitudinal direction, the atoms have an optical depth of 32 in the  $|1\rangle \rightarrow |3\rangle$  transition. The pump laser (780 nm,  $\omega_p$ ) is 80 MHz blue detuned from the transition  $|1\rangle \rightarrow |4\rangle$ , and the coupling laser (795 nm,  $\omega_c$ ) is on resonance with the transition  $|2\rangle \rightarrow |3\rangle$ . The linear polarized pump laser beam, with a  $1/e^2$  diameter of 1.8 mm, is equally split into two beams after a half-wave plate and the first polarization beam splitter (PBS1). These two beams, with opposite circular polarizations ( $\sigma^+$  and  $\sigma^-$ ) after two quarter-wave plates, then intersect at the MOT with an angle of  $\pm 2.5^\circ$  to the longitudinal axis. Similarly, the two coupling laser beams after PBS2 with opposite circular polarizations overlap with the two pump beams from opposite directions. In the presence of these two pairs of counterpropagating pump-coupling beams, phase-matched Stokes ( $\omega_s$ ) and anti-Stokes ( $\omega_{as}$ ) paired photons are produced along the longitudinal axis and coupled into two opposing single-mode fibers (SMFs). In each SFWM path, the polarizations of the Stokes and anti-Stokes photons follow those of the corresponding pump and coupling field, respectively. The two SMF spatial modes are focused at the MOT center with a  $1/e^2$  diameter of 0.4 mm. After two narrow-band filters ( $F_1$  and  $F_2$ , 0.5 GHz bandwidth), the photons are detected by two single-photon counter modules (SPCM, Perkin Elmer SPCM-4Q4C) and analyzed by a time-to-digital converter (Fast Comtec P7888) with a time bin width of 1 ns. Two sets of quarter-wave plates, half-wave plates, and PBSs are inserted for measuring polarization correlation and quantum state tomography.

To obtain the polarization entanglement, we must stabilize the phase difference between the two SFWM spatial paths. This is achieved by injecting a reference laser beam (795 nm, 110 MHz blue detuned from the transition  $|2\rangle \rightarrow |3\rangle$ ) from the second input of PBS2. The two reference beams split after PBS2 are then recombined after PBS1 and detected by a photodetector (a half-wave plate and a PBS are used to obtain the interference), as shown in Fig. 1. This is a standard Mach-Zehnder interferometer to

the reference laser. Locking the phase difference of the two arms of the Mach-Zehnder interferometer with a feedback electronics stabilizes the phase of the two SFWM paths (see Supplemental Material [19]). To avoid interaction with the cold atoms, the reference beams are slightly shifted away from the pump-coupling beams but pass through the same optical components.

Following the perturbation theory [11], the produced two-photon state can be described as (see Supplemental Material [19] for the derivation)

$$|\Psi\rangle = L \int \kappa(\omega_{as}) \text{sinc} \left[ \frac{\Delta k(\omega_{as})L}{2} \right] |\omega_s = \omega_p + \omega_c - \omega_{as}\rangle \times |\omega_{as}\rangle d\omega_{as} \otimes \frac{1}{\sqrt{2}} (|\sigma_p^1\rangle_s |\sigma_c^1\rangle_{as} + e^{i\phi} |\sigma_p^2\rangle_s |\sigma_c^2\rangle_{as}), \quad (1)$$

which shows hyperentanglement in frequency (continuous) and polarization (discrete). The upper indices (1 and 2) represent the two SFWM spatial paths.  $\Delta k(\omega_{as})$  is the phase mismatching, and  $\kappa(\omega_{as})$  is the nonlinear parametric coupling coefficient.  $\kappa(\omega_{as}) \text{sinc}[\Delta k(\omega_{as})L/2]$  determines the photon spectrum.  $\phi$  is the phase difference between the two SFWM paths. Equation (1) can also be rewritten in the time and polarization domains

$$|\Psi(t_s, t_{as})\rangle = \psi(t_{as} - t_s) e^{-i(\bar{\omega}_s t_{as} + \bar{\omega}_s t_s)} \times \otimes \frac{1}{\sqrt{2}} (|\sigma_p^1\rangle_s |\sigma_c^1\rangle_{as} + e^{i\phi} |\sigma_p^2\rangle_s |\sigma_c^2\rangle_{as}), \quad (2)$$

where  $t_s$  and  $t_{as}$  are the detection time of the Stokes and anti-Stokes photons, respectively.  $\bar{\omega}_s$  and  $\bar{\omega}_{as}$  are their central frequencies, respectively. The time-domain wave function  $\psi(t_{as} - t_s)$  results from the frequency entanglement ( $\omega_s = \omega_p + \omega_c - \omega_{as}$ ) and is the Fourier transform of the two-photon joint spectrum. Meanwhile, as shown in Eqs. (1) and (2), the polarization entanglement can be

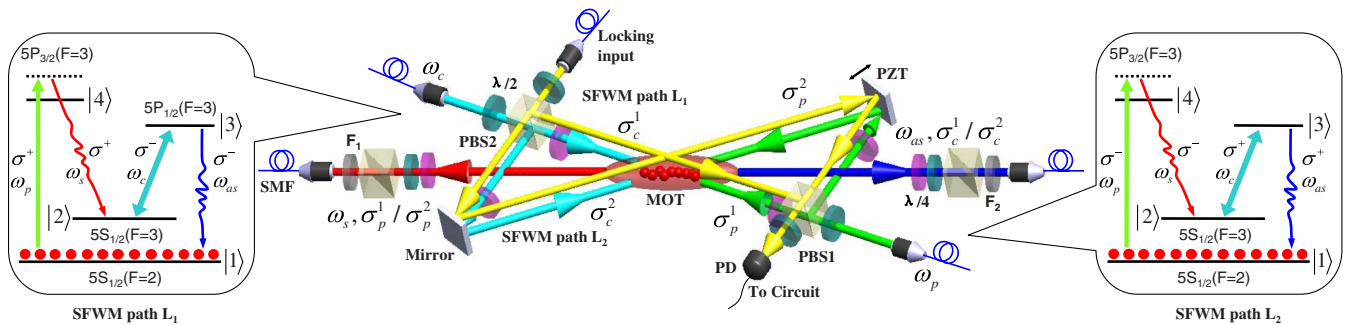


FIG. 1 (color online). Experimental setup for producing subnatural-linewidth polarization-entangled photon pairs. The polarization entanglement is created by the quantum interference of the two spatially symmetric SFWM processes driven by two counterpropagating pump-coupling beams ( $L_1$  and  $L_2$ ). The phase difference of the two SFWM paths is stabilized by locking the reference laser in the Mach-Zehnder interferometer, whose output is detected by a photodetector (PD). To avoid interaction with the cold atoms, the reference beams are slightly shifted away from the pump-coupling beams but pass through the same optical components. The inserted energy level diagrams are two possible SFWM channels for  $L_1$  and  $L_2$ , respectively. PZT: Piezoelectric transducer.

manipulated by controlling the pump-coupling polarizations and phase difference.

We first characterize the two-photon nonclassical correlation in the time domain. Figures 2(a)–2(c) show the two-photon coincidence counts as functions of the relative time delay ( $\tau = t_{as} - t_s$ ) with the polarization configurations  $\sigma_s^+ \sigma_{as}^-$ ,  $\sigma_s^- \sigma_{as}^+$ , and  $\sigma_s^+ \sigma_{as}^- + \sigma_s^- \sigma_{as}^+$ , respectively. We carefully balance the pump and coupling laser powers on the two SFWM paths to make their correlation indistinguishable in the time domain for achieving the maximally polarization-entangled states. At each path, the pump beam has a power of  $8 \mu\text{W}$  and the coupling beam of  $2 \text{ mW}$ . As shown in Fig. 2, these paired photons have a temporal correlation length of  $300 \text{ ns}$ . Normalizing the coincidence counts to the accidental uncorrelated background counts, we obtain the normalized cross correlation  $g_{s,as}^{(2)}(\tau)$  with a peak value of 35 at  $\tau = 25 \text{ ns}$ . With measured autocorrelations  $g_{s,s}^{(2)}(0) = g_{as,as}^{(2)}(0) \approx 2.0$ , we confirm that the Cauchy-Schwartz inequality  $[g_{s,as}^{(2)}(\tau)]^2 \leq g_{s,s}^{(2)}(0)g_{as,as}^{(2)}(0)$  is violated by a factor of 306, which clearly indicates the quantum nature of the paired photons. With an integration time bin of  $300 \text{ ns}$ , the normalized cross correlation has a reduced peak value of 10, which still violates the Cauchy-Schwartz inequality by a factor of 25. The solid curves in Figs. 2(a)–2(c) are calculated from Eq. (2). The nearly perfect agreement between the theory and experiment indirectly verifies the time-frequency entanglement. The shorter correlation time in Fig. 2(c) compared to that in

Figs. 2(a) and 2(b) is caused by the addition of the powers from the two coupling beams that widen the EIT and biphoton bandwidth. The coherence time of about  $300 \text{ ns}$  corresponds to an estimated bandwidth of  $2.9 \text{ MHz}$  (also confirmed from the theory). The photon bandwidth can be further reduced by lowering the coupling laser power to narrow the EIT window. Figure 2(d) shows the measured correlation time versus the coupling laser power. With  $0.13 \text{ mW}$  coupling laser power, we obtain a coherence time of up to  $900 \text{ ns}$ , which corresponds to a bandwidth of about  $0.8 \text{ MHz}$ . The solid curve in Fig. 2(d) is also obtained with Eq. (2).

We next demonstrate that all four polarization-entangled Bell states can be realized by locking the phase  $\phi$  as well as properly choosing the polarizations of the coupling and pump laser beams. As shown in Eq. (2), locking the phase difference  $\phi$  as  $0$  or  $\pi$  and setting  $\sigma_p^1 = \sigma_c^2 = \sigma^+$ ,  $\sigma_c^1 = \sigma_p^2 = \sigma^-$ , we can produce two polarization-entangled Bell states:

$$|\Psi^\pm\rangle = \frac{1}{\sqrt{2}}(|\sigma_s^+ \sigma_{as}^- \rangle \pm |\sigma_s^- \sigma_{as}^+ \rangle). \quad (3)$$

Similarly, by setting  $\sigma_p^1 = \sigma_c^1 = \sigma^+$ ,  $\sigma_p^2 = \sigma_c^2 = \sigma^-$ , we obtain other two Bell states:

$$|\Phi^\pm\rangle = \frac{1}{\sqrt{2}}(|\sigma_s^+ \sigma_{as}^+ \rangle \pm |\sigma_s^- \sigma_{as}^- \rangle). \quad (4)$$

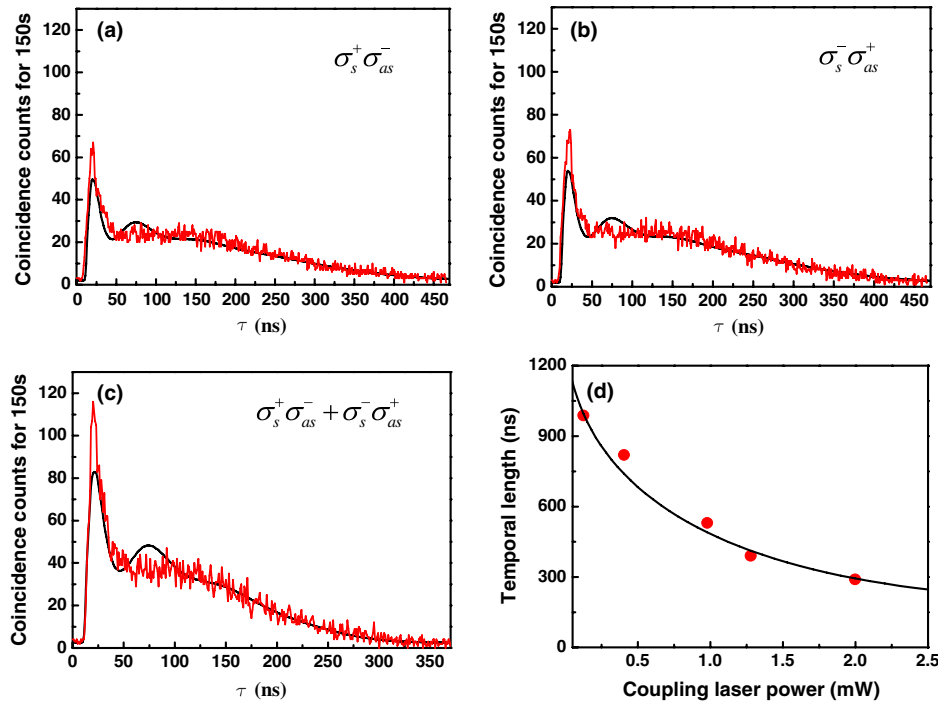


FIG. 2 (color online). (a)–(c) Two-photon coincidence counts as a function of the relative time delay between the Stokes and anti-Stokes photons. (a) Path 1:  $\sigma_p^1 = \sigma^+$  and  $\sigma_c^1 = \sigma^-$ ; path 2: blocked. (b) Path 1: blocked; path 2:  $\sigma_p^2 = \sigma^-$  and  $\sigma_c^2 = \sigma^+$ . (c) Both paths are present. (d) The temporal length of the paired photons as a function of the coupling laser power. All the black lines are theoretical plots.

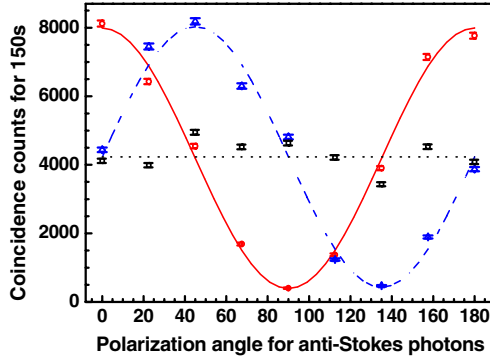


FIG. 3 (color online). Polarization correlation of the paired Stokes and anti-Stokes photons at  $\phi = 0$ . The polarization angles for Stokes photons are set at  $0^\circ$  (red solid line and circle) and  $-45^\circ$  (blue dashed line and triangle). The black dotted line and squares are the data taken without stabilizing  $\phi$ .

Figure 3 displays the measured two-photon polarization correlations for  $|\Psi^+\rangle$  by locking  $\phi = 0$ . The coincidence counts are integrated from  $\tau = 0$  to 300 ns for a total measurement time of 150 s. The circle data ( $\circ$ , red line) are collected by fixing the Stokes photon polarization angle at  $0^\circ$  and the triangle data ( $\Delta$ , blue line) at  $-45^\circ$ . Other parameters during the measurement remain the same as those for Fig. 2(c). The solid cosine- and sine-wave curves are the theoretical fits with adjustable background and amplitude parameters. We obtain the visibility  $V = 89.3\%$ , which is beyond the requirement of  $1/\sqrt{2}$  for violating the Bell-Cluser-Horne-Shimony-Holt (Bell-CHSH) inequality [20]. For comparison, we plot the data without locking the phase as the square points ( $\square$ , black line) which shows no quantum interference.

To obtain a complete characterization of the polarization entanglement, we also make a quantum state tomography to determine the density matrix following the maximum likelihood estimation method [21,22]. With two additional quarter-wave plates, the circular polarization basis  $|\sigma_s^+ \sigma_{as}^- \rangle$ ,  $|\sigma_s^- \sigma_{as}^+ \rangle$ ,  $|\sigma_s^+ \sigma_{as}^+ \rangle$ , and  $|\sigma_s^- \sigma_{as}^- \rangle$  can be converted into linear polarization basis  $|HH\rangle$ ,  $|VV\rangle$ ,  $|HV\rangle$ , and  $|VH\rangle$ . Then we use a half-wave plate followed by a PBS as the polarization selector. The density matrix is constructed from the coincidence counts at 16 independent projection states (see Supplemental Material [19]). The graphical representations of the obtained density matrix for  $|\Psi^\pm\rangle$  and  $|\Phi^\pm\rangle$  are shown in Fig. 4, from which we obtain the fidelities of 93.6%, 91.8%, 92.9%, and 95.2%, respectively. We also use the density matrix to test the violation of the Bell-CHSH inequality ( $S > 2$ ) and get the values  $S = 2.23 \pm 0.025$ ,  $2.19 \pm 0.026$ ,  $2.3 \pm 0.02$ , and  $2.39 \pm 0.026$  for the obtained four Bell states.

Now, we turn to the brightness of our photon source. For the data shown in Fig. 2(c), by taking into account the fiber coupling efficiency (70%), filter transmission (70%), detector quantum efficiency (50%), and duty cycle (10%), our

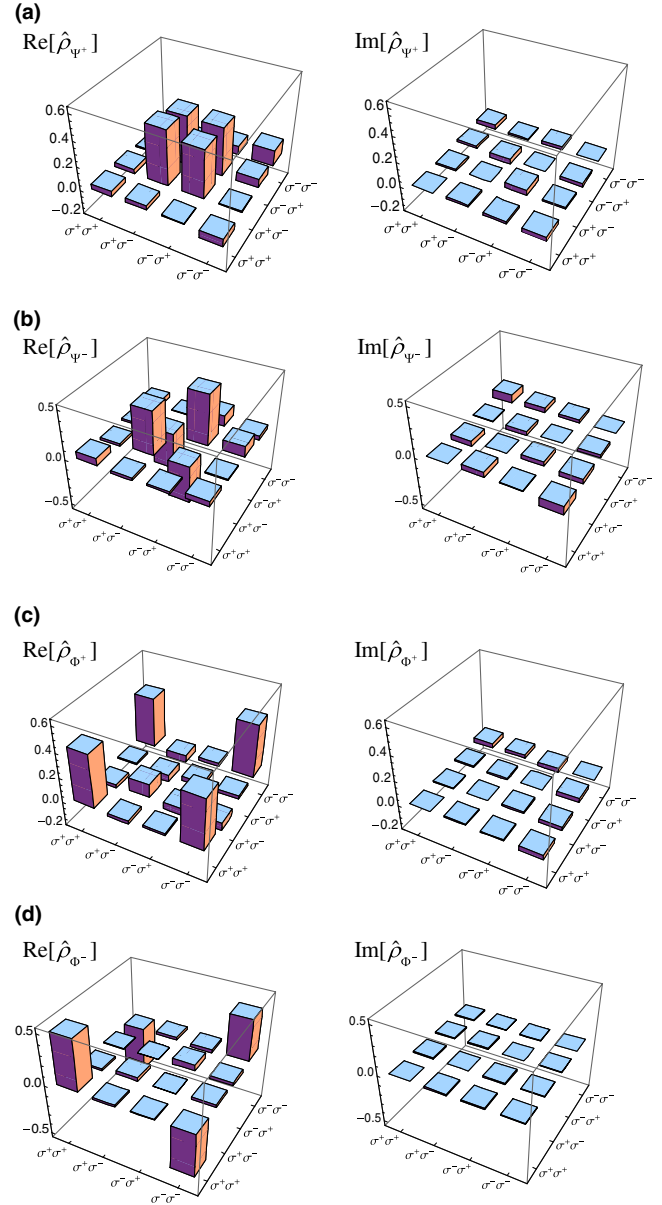


FIG. 4 (color online). Tomography measurement results of the photon pairs at the target polarization-entangled Bell states (a)  $|\Psi^+\rangle$ , (b)  $|\Psi^-\rangle$ , (c)  $|\Phi^+\rangle$ , and (d)  $|\Phi^-\rangle$ .

photon source spontaneously generates about 9800 photon pairs per second. With the pump power of  $16 \mu\text{W}$  and a linewidth of 2.9 MHz, we estimate a spectrum brightness of  $3400 \text{ s}^{-1} \text{ MHz}^{-1}$  and the normalized spectrum brightness of  $213000 \text{ s}^{-1} \text{ MHz}^{-1} \text{ mW}^{-1}$ . We can further increase the photon pair generation rate by increasing the pump laser power. Figure 5 shows the dependence of the visibility of the polarization correlation to the photon pair generation rate. The visibility is estimated from  $V = (g_{s,as}^{(2)} - 1)/(g_{s,as}^{(2)} + 1)$  [23,24]. As long as the generation rate is less than  $4 \times 10^4 \text{ s}^{-1}$  (here the averaged normalized cross correlation is under consideration), the visibility is larger

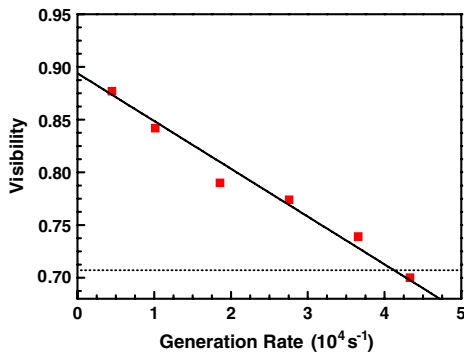


FIG. 5 (color online). Visibility versus the biphoton generation rate. The solid line is the linear fit. The dashed line marks the boundary for violating the Bell-CHSH inequality.

than  $1/\sqrt{2}$ , which is the boundary to violate the Bell-CHSH inequality.

In summary, we have demonstrated an efficient experimental scheme for producing subnatural-linewidth photon pairs with polarization entanglement. The polarization entanglement results from the interference between the two SFWM spatial paths. By stabilizing the phase difference between these two paths and setting properly the driving laser polarizations, we produce all four Bell states, confirmed by the quantum state tomography measurements. Their long coherence time (up to 900 ns) and narrow bandwidth (about 1 MHz) make them a promising entangled photon source for interacting with rubidium atomic quantum nodes.

We thank J. F. Chen and C. Liu for their helpful discussion. This work was supported by the NSFC (Grants No. 11104085, No. 11125417, and No. 61378012), the Major Research Plan of the NSFC (Grant No. 91121023), the SKPBR of China (Grants No. 2011CB922104 and No. 2011CBA00200), the FOYTHEG (Grant No. Yq2013050), the PRNPGZ (Grant No. 2014010), and the PCSIRT (Grant No. IRT1243). S. D. was supported by Hong Kong Research Grants Council (Project No. HKU8/CRF/11G).

\*yanhui@snu.edu.cn

†slzhunju@163.com

- [1] L. M. Duan, M. D. Lukin, J. I. Cirac, and P. Zoller, *Nature (London)* **414**, 413 (2001).  
 [2] H. J. Kimble, *Nature (London)* **453**, 1023 (2008).

- [3] Z. Y. Ou and Y. J. Lu, *Phys. Rev. Lett.* **83**, 2556 (1999).  
 [4] H. Wang, T. Horikiri, and T. Kobayashi, *Phys. Rev. A* **70**, 043804 (2004).  
 [5] X. H. Bao, Y. Qian, J. Yang, H. Zhang, Z.-B. Chen, T. Yang, and J.-W. Pan, *Phys. Rev. Lett.* **101**, 190501 (2008).  
 [6] M. Scholz, L. Koch, and O. Benson, *Phys. Rev. Lett.* **102**, 063603 (2009).  
 [7] J. Fekete, D. Rieländer, M. Cristiani, and H. de Riedmatten, *Phys. Rev. Lett.* **110**, 220502 (2013).  
 [8] M. Förtsch, J. U. Fürst, C. Wittmann, D. Strekalov, A. Aiello, M. V. Chekhova, C. Silberhorn, G. Leuchs, and C. Marquardt, *Nat. Commun.* **4**, 1818 (2013).  
 [9] H. Zhang, X. M. Jin, J. Yang, H. N. Dai, S. J. Yang, T. M. Zhao, J. Rui, Y. He, X. Jiang, F. Yang, G. S. Pan, Z. S. Yuan, Y. Deng, Z. B. Chen, X. H. Bao, S. Chen, B. Zhao, and J. W. Pan, *Nat. Photonics* **5**, 628 (2011).  
 [10] S. W. Du, P. Kolchin, C. Belthangady, G. Y. Yin, and S. E. Harris, *Phys. Rev. Lett.* **100**, 183603 (2008).  
 [11] S. W. Du, J. M. Wen, and M. H. Rubin, *J. Opt. Soc. Am. B* **25**, C98 (2008).  
 [12] S. Y. Zhou, S. C. Zhang, C. Liu, J. F. Chen, J. M. Wen, M. M. T. Loy, G. K. L. Wong, and S. W. Du, *Opt. Express* **20**, 24124 (2012).  
 [13] S. Zhang, J. F. Chen, C. Liu, M. M. T. Loy, G. K. L. Wong, and S. Du, *Phys. Rev. Lett.* **106**, 243602 (2011).  
 [14] S. Zhang, C. Liu, S. Zhou, C.-S. Chuu, M. M. T. Loy, and S. Du, *Phys. Rev. Lett.* **109**, 263601 (2012).  
 [15] Y. C. Chen, C. W. Lin, and I. A. Yu, *Phys. Rev. A* **61**, 053805 (2000).  
 [16] H. Yan, S. C. Zhang, J. F. Chen, M. M. T. Loy, G. K. L. Wong, and S. W. Du, *Phys. Rev. Lett.* **106**, 033601 (2011).  
 [17] D. Matsukevich and A. Kuzmich, *Science* **306**, 663 (2004).  
 [18] S. Zhang, J. F. Chen, C. Liu, S. Zhou, M. M. T. Loy, G. K. L. Wong, and S. Du, *Rev. Sci. Instrum.* **83**, 073102 (2012).  
 [19] See Supplemental Material at <http://link.aps.org/supplemental/10.1103/PhysRevLett.112.243602> for the derivation of Eqs. (1) and (2), the method to lock the phase  $\phi$ , and the density matrix results of the four Bell states.  
 [20] J. F. Clauser, *Phys. Rev. D* **9**, 853 (1974).  
 [21] A. G. White, D. F. V. James, P. H. Eberhard, and P. G. Kwiat, *Phys. Rev. Lett.* **83**, 3103 (1999).  
 [22] D. F. V. James, P. G. Kwiat, W. J. Munro, and A. G. White, *Phys. Rev. A* **64**, 052312 (2001).  
 [23] H. de Riedmatten, J. Laurat, C. W. Chou, E. W. Schomburg, D. Felinto, and H. J. Kimble, *Phys. Rev. Lett.* **97**, 113603 (2006).  
 [24] J. K. Thompson, J. Simon, H. Q. Loh, and V. Vuletić, *Science* **313**, 74 (2006).